# Versatile electrical behavior of $1T$-$TiS_2$ elucidated from a theoretical study

Adrien Stoliaroff, Camille Latouche, and Stéphane Jobic*

*Institut des Matériaux Jean Rouxel (IMN), Université de Nantes, CNRS, 2 rue de la Houssinière, BP 32229, 44322 Nantes cedex 3, France*

(Received 24 January 2019; revised manuscript received 25 March 2019; published 16 April 2019)

Herein we report the formation energies of native point defects in $1T$-$TiS_2$ material. In the present study we used one of the most refined models, e.g., a global hybrid density functional with dispersion corrections for all the calculations. The stability domain of $1T$-$TiS_2$ was thoroughly investigated. We demonstrate unambiguously that the most stable defect is titanium interstitial in octahedral site in the van der Waals gap. Indeed, this simple defect can explain the distinguishable electric behavior of $TiS_2$ reported in the litterature, i.e., nondegenerated semiconductor (SC) or semimetal (SM) depending on the synthesis conditions. Simulated defect concentrations vs synthesis temperature are also provided and the SC-SM transition is discussed.

DOI: 10.1103/PhysRevB.99.165122

## I. INTRODUCTION

Transition metal dichalcogenides (TMD) $MQ_2$, with $M$ a transition metal and $Q$ a chalcogen ($Q$ = S, Se, Te), are currently a focus of a large number of solid-state scientists due to the peculiar physics taking place in these layered compounds. The properties of both bulk and single layers nowadays attract interest as they may significantly differ [1–4]. The exploration of the properties of such materials opens the way for the development of devices [5–7] in various fields such as biomedical applications [8–10] or energy storage [11–13].

Among this family of compounds, titanium disulfide $TiS_2$ has been studied throughout the past [14–23] and more studies on this material have kept coming in ever since. It was first of interest as an intercalation material for lithium batteries [24–29], then with other species like cesium [30,31], ionic liquids [32], mercury [29,33–39], silver [40–42], and mostly sodium [25,43–45]. The search was extended to other applications such as hydrogen production [46] and storage [47] or, recently, thermoelectricity [48–51]. However, despite the apparent simplicity of the material–only three atoms per unit cell–there is still an ongoing controversy about its bulk electronic properties. Some experimental measurements have concluded that it is a low band-gap semiconductor [21,52] whereas others have described it as a semimetal [18,53]. The dispute goes on when one looks at the theoretical side of the question, with some simulations obtaining a band-gap [54–57] and others a semimetallic behavior [53,58,59]. There is still active research on this material, both from a fundamental point of view [60–64] and looking for applications [65,66].

In a recent study [67], we used refined models ranging from the generalized gradient approximation (GGA) to many-body perturbation theory (GW) to look at the electronic properties of ideal $TiS_2$. This led us to conclude that the bulk material $1T$-$TiS_2$ is a semiconductor with a quite low band gap ($\approx$0.7 eV), a behavior which we confirmed can be switched to semimetallic by applying pressure, as reported by Xu *et al.* [59]. It also pointed out PBE0 with dispersion correction as the model exhibiting the best accuracy vs computational time ratio. However, it has been repeatedly pointed out in the literature that obtaining stoichiometric $TiS_2$ experimentally is a daunting task [21,52]. Defects are known to greatly affect a material's properties and titanium disulfide appeared to be particularly defect sensitive, which could explain the discrepancies observed on synthesized $TiS_2$. This prompted us to study intrinsic point defects of $TiS_2$ using a hybrid density functional. This approach is still rare for point defect investigations in bulk materials, and the few studies reaching this level of theory mainly rely on screened hybrid functionals [68–72].

Experimentally, an overstoichiometry in titanium due to interstitials located inside the van der Waals gap has long been suspected [52,73] but not yet fully proven.

In this paper, it is demonstrated that vacancies of titanium are not expected whatever the synthesis conditions. Conversely, an overstoichiometry in titanium with respect to sulfur is anticipated due to the low $Ti_i$ formation enthalpy. The sulfur atmosphere (i.e., S-rich/Ti-poor vs S-poor/Ti-rich) strongly impacts the Ti interstitial concentration and subsequently the positioning of the Fermi level and the semiconducting or semimetallic behavior of $TiS_2$.

## II. COMPUTATIONAL DETAILS

The calculations were performed on a $4 \times 2 \times 2$ supercell of 48 atoms using PBE0 [74,75] hybrid functional together with a projector-augmented waves (PAW) scheme as implemented in VASP [76–79]. One needs to stress out that the hybrid functional was used for all calculations throughout the study, including geometrical relaxations. Grimme semiempirical dispersion effect with Becke-Johnson damping factors [80–82] were included in order to account for the van der Waals interactions as discussed in our previous paper [67] and the literature [61]. An energy cutoff of 400 eV was chosen. The first Brillouin zone was sampled with a Monkhorst Pack scheme [83] on a $3 \times 3 \times 3$ mesh. The convergence criterion regarding forces was set to $1.10^{-2}$ eV/Å due to high

*stephane.jobic@cnrs-imn.fr

 

computational costs and at $1.10^{-5}$ eV for the convergence of the self-consistent cycle. All post-treatments were performed with the PYDEF 2.0 software [84,85].

## III. DEFECT FORMATION ENTHALPIES AND CONCENTRATIONS METHODOLOGIES

As the variations of volume in the case of diluted defects are negligible [86], the formation enthalpy of defects can be assimilated to the formation enthalpy. One may compute the formation enthalpy $\Delta H^{D,q}_{\text{form}}$ of a defect $D$ in a state of charge $q$ as a linear function of the chemical potential of the electron reservoir (Fermi level) $\mu_{E_F}$ as expressed in the following equation [87–91]:

$$\Delta H^{D,q}_{\text{form}}(\mu_{E_F}) = E^{D,q}_{\text{total}} - E^{\text{host}}_{\text{total}} + \sum_i n_i\left(\mu^0_i + \Delta\mu_i\right) + q\left(E^{\text{host}}_{\text{VBM}} + \mu_{E_F}\right) + \text{corr}(D,q) \quad (1)$$

where $E^{D,q}_{\text{total}}$ is the energy of the defect supercell, $E^{\text{host}}_{\text{total}}$ is the total energy of the perfect cell, $E^{\text{host}}_{\text{VBM}}$ is the energy of the valence-band maximum (VBM) in the ideal structure taken as a reference for the value of the Fermi level, $\mu_i$ is the chemical potential of the $i$th chemical element defined as $\mu^0_i + \Delta\mu_i$ ($\Delta\mu_i < 0$), i.e., the potential of the chemical element $i$ in its standard phase (most thermodynamically stable in normal conditions), and the deviation $\Delta\mu_i$ from this reference. corr$(D,q)$ corrects spurious effects introduced by the supercell model [92] (see Supplemental Material for a description of the energy corrections in the point defect model).

A key quantity is the transition level $\epsilon_{(q_0,q_1)}$ given as

$$\epsilon_{(q_0,q_1)} = -\frac{\Delta H^{D,q_1}_{\text{form}}(0) - \Delta H^{D,q_0}_{\text{form}}(0)}{q_1 - q_0}. \quad (2)$$

It is the level at which the formation enthalpies of $q_1$ and $q_0$ are equal $\Delta H^{D,q_0}(\epsilon_{(q_0,q_1)}) = \Delta H^{D,q_1}(\epsilon_{(q_0,q_1)})$. In the case of a defect with only two charge states, this is the value of $\mu_{E_F}$ at which the population of defect $D$ charged $q_0$ is as large as the population $D$ charged $q_1$.

By solving the charge neutrality equation (3), one can obtain the concentration of defects at equilibrium via the position of the Fermi level in the band gap at crystal growth $E^{\text{gr}}_F$. We assume that the material is then quenched from synthesis to room temperature so that the total concentration $n_D$ remains constant once cooled down. The neutrality is expressed as

$$n_{h^+}\left(E^{\text{gr}}_F\right) - n_{e^-}\left(E^{\text{gr}}_F\right) + \sum_{\substack{D\in\{\text{defects}\}\\ q\in\{q(D)\}}} q n_{D,q}\left(E^{\text{gr}}_F\right) = 0, \quad (3)$$

where $n_{e^-}$ and $n_{h^+}$ are the free electrons/holes temperature-dependent populations as functions of $E_F$, given as

$$n_{h^+}(E_F) = \int_{-\infty}^{E_{\text{VBM}}} g_{h^+}(\mu)[1 - f_{\text{FD}}(\mu - E_F)]d\mu \quad (4)$$

$$n_{e^-}(E_F) = \int_{E_{\text{CBM}}}^{+\infty} g_{e^-}(\mu) f_{\text{FD}}(\mu - E_F)d\mu, \quad (5)$$

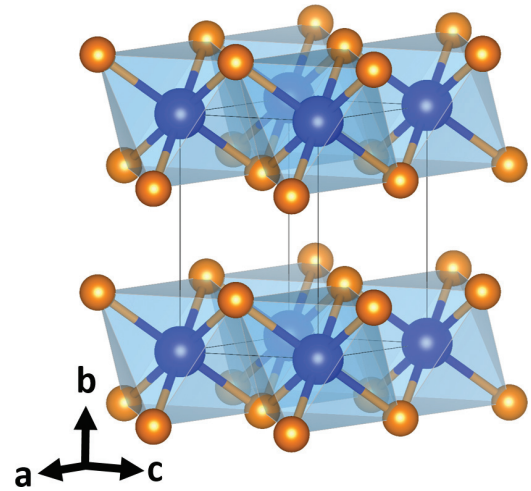


FIG. 1. $TiS_2$ conventional cell of $CdI_2$ trigonal structure [space group $P\bar{3}m1$ (164)] exhibiting a van der Waals gap separating [$TiS_6$] sheets.

where $f_{\text{FD}}(E)$ is the Fermi-Dirac distribution,

$$f_{\text{FD}}(\mu - E_F) = \frac{1}{1 + e^{(\mu - E_F)/k_BT}}, \quad (6)$$

and $g(E)$ is the density of states,

$$\forall i \in \{e^-, h^+\}, g_i(\mu) = \frac{1}{4\pi^2}\left(\frac{2m^*_i}{\hbar^2}\right)^{3/2}\sqrt{\mu}. \quad (7)$$

## IV. RESULTS AND DISCUSSION

### A. Structure and electronic structure

$TiS_2$ crystallizes in the $CdI_2$ trigonal structure [space group $P\bar{3}m1$ (164)] with Ti and S atoms in $1a$ and $2d$ Wyckoff positions [(0,0,0), $(\frac{1}{3},\frac{2}{3},z)$ with $z \simeq \frac{1}{4}$, respectively; see Fig. 1] [93]. $TiS_2$ slabs are built upon [$TiS_6$] edge-sharing polyhedra and octahedral sites in the van der Waals gap are vacant in the ideal 1:2 material.

The optimized model structure nicely agrees with experiment as previously reported [67] and is therefore not discussed herein. The band diagram obtained in PBE0-GD3BJ is displayed in Fig. 2. The electronic band structure of ideal bulk

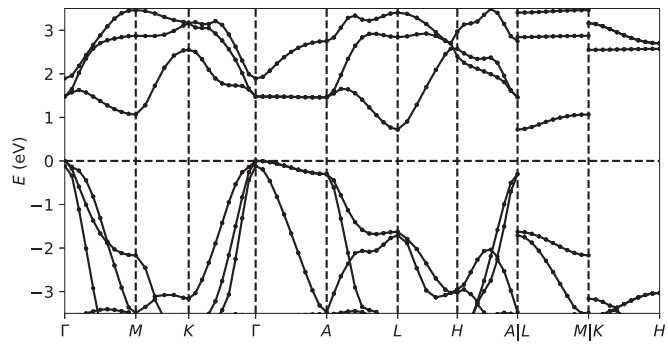


FIG. 2. $TiS_2$ band diagram obtained with PBE0-GD3BJ functional [$\Gamma(0,0,0)$, $M(\frac{1}{2},0,0)$, $K(\frac{1}{3},\frac{1}{3},0)$, $A(0,0,\frac{1}{2})$, $L(\frac{1}{2},0,\frac{1}{2})$, $H(\frac{1}{3},\frac{1}{3},\frac{1}{2})$].

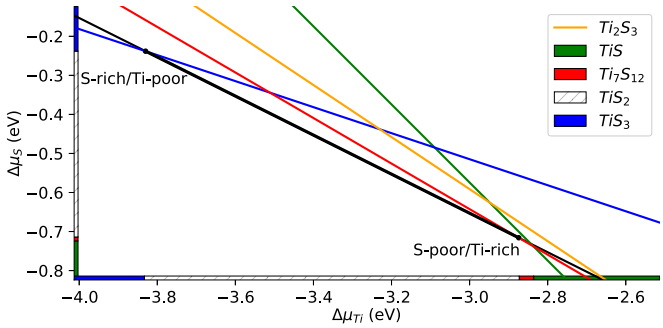


FIG. 3. $TiS_2$ stability domain with respect to competitive phases and the chemical potentials in Ti and S. The $TiS_2$ line is defined by the equation $\Delta H_f(TiS_2) = \Delta\mu_{Ti} + 2\Delta\mu_S$. The S-rich/Ti-poor limit is defined by the intersection with the formation enthalpy line of $TiS_3$ (blue) and the S-poor/Ti-rich frontier with $Ti_7S_{12}$ (red).

$TiS_2$ computed at this level of theory exhibits a small energy gap of $\simeq$0.7 eV. The maximum of the valence band is at the $\Gamma$ point whereas the minimum of the conduction band is located at $L$. Both the valence band and the conduction band are quite dispersed, leading to low effective masses of charge carriers, and expected high carrier mobilities.

### B. Stability domain and chemical potentials

The ICSD crystallographic database [94,95] includes roughly 20 different structure types for the Ti-S system. We filtered these phases to keep only those with the Ti/S ratio the closest to $\frac{1}{2}$ (i.e., chemical compositions which frame $TiS_2$). However, experimental structures may correspond to metastable phases which should not be included in our thermodynamic stability calculation. Thus, we confronted the ICSD structures with high-throughput calculations [96–98] to retain only thermodynamically stable phases. Reported Ti-S compounds with a Ti/S ratio close to $\frac{1}{2}$ count TiS, $Ti_2S_3$, $TiS_2$ the object of the study and $TiS_3$ [96–99]. The region between $TiS_2$ and TiS is ill defined. Indeed, Murray *et al.* claimed the existence of several metastable phases at this limit [99]. High throughput calculations identified another stable composition in this region, $Ti_7S_{12}$ ($Ti_{1.167}S_2$), obtained by stabilizing two titanium interstitials in the van der Waals gaps of a $3 \times 2 \times 2$ $TiS_2$ supercell. This hypothetical compound has not been observed yet, however Tronc *et al.* [100] reported a $R\bar{3}m$ (166) $Ti_{1.17}S_2$ structure with disorders whose stoichiometry might correspond to the $\frac{7}{12}$ Ti/S ratio. The latter structure cannot be used in an *ab initio* calculation because it exhibits irrational partial occupancies. We used $Ti_7S_{12}$ from the Materials Project [96–98] to model the unknown region S-poor/Ti-rich region. Upon computations of all nonfaulted reported stoichiometries, it is then possible to obtain the stability diagram of $TiS_2$ (Fig. 3).

The thermodynamic stability domain is drawn in a ($\Delta\mu_{Ti}$, $\Delta\mu_S$) chemical potential diagram. For each compound competing against $TiS_2$ during synthesis, one can plot the line defined by its formation enthalpy [see Eq. (7) of the Supplemental Material for stability domain equations [92]]. Hence, to any given value of $\Delta\mu_{Ti}$ corresponds a unique value of $\Delta\mu_S$ and *vice versa*. The ranges of each stability domain can be read on each axis and are summarized for $TiS_2$ in Table I. Hereafter, we will refer to a S-rich/Ti-poor (S-poor/Ti-rich) atmosphere for the limit of apparition of $TiS_3$ ($Ti_7S_{12}$).

TABLE I. Computed extrema chemical potentials to form $TiS_2$ ($\mu_S^0 = -5.976$ eV and $\mu_{Ti}^0 = -10.987$ eV).

| (eV) | $\mu_S$ ($\Delta\mu_S$) | $\mu_{Ti}$ ($\Delta\mu_{Ti}$) |
|---|---|---|
| S-poor/Ti-rich | −6.692 (−0.716) | −13.862 (−2.875) |
| S-rich/Ti-poor | −6.214 (−0.238) | −14.817 (−3.830) |

$TiS_3$ is the most stable material until ($\Delta\mu_{Ti} = -3.83$ eV, $\Delta\mu_S = -0.24$ eV). The intersection of $TiS_3$ and $TiS_2$ formation enthalpies defines the called S-rich/Ti-poor limit of the stability domain of $TiS_2$. Moreover, when one increases $\mu_{Ti}$ (decreases in absolute value) and decreases $\mu_S$ (increases in absolute value) down to ($\Delta\mu_{Ti} = -2.88$ eV, $\Delta\mu_S = -0.72$ eV), the most stable phase is not anymore $TiS_2$. As discussed before, this quite uncertain region is modelled by considering $Ti_7S_{12}$ as the most stable phase. Thus, because of the presence of $TiS_3$ and $Ti_7S_{12}$, the frontiers of the stability domain of $TiS_2$ are never delimited by Ti or S reference thermodynamic phase (Ti metal and crystal $\alpha - S_8$, respectively) which induces a systematic deviation of chemical potentials from the standard potentials.

### C. Defects considered

Intrinsic point defects only involve the atoms of the lattice, as opposed to extrinsic defects which may result from the (sometimes unintentional) addition of other chemical species. They are inherently present for thermodynamic reasons, however they are so diluted they do not affect the global structure of the material which still appears unchanged with X-ray diffraction. Thus they should be distinguished from solid solution. Herein, intrinsic point defects of $TiS_2$ were investigated, namely titanium interstitials $Ti_i$, titanium vacancies $V_{Ti}$, and sulfur vacancies $V_S$. The compound is known to exhibit naturally an overstoichiometry in titanium [21], thus sulfur interstitials were not considered. Titanium interstitials located in the van der Waals gap in a tetrahedral environment were also considered and found to have a much higher formation enthalpy than the analogous defect in an octahedral environment ($\approx$1 eV, which corresponds to $\frac{[Ti_i(T_d)]}{[Ti_i(O_h)]} = e^{-\Delta H/k_B T} < 6 \times 10^{-5}$ for $T = 1200$ K, for instance). Thus it is neglected for the rest of the study.

### D. Defect formation enthalpies

The resulting defect formation enthalpies vs Fermi level are shown in Fig. 4. As expected in both conditions (S-rich/Ti-poor and S-poor/Ti-rich), the formation of $V_{Ti}$ is unlikely due to its rather high defect formation enthalpy (>2 eV considering both atmospheres) without shallow transition level ($\epsilon_{(0,-4)} = 0.45$ eV). Because of its high formation enthalpy, $V_{Ti}$ can only be expected in tiny concentrations in the material and thus will not play a leading role in the electronic properties.

The formation enthalpy of $V_S$ varies between 1.36 eV (at $\mu_{E_F} = 0$ eV) and 2.55 eV ($\mu_{E_F} > \epsilon_{(+2,0)}$) in S-rich/Ti-poor

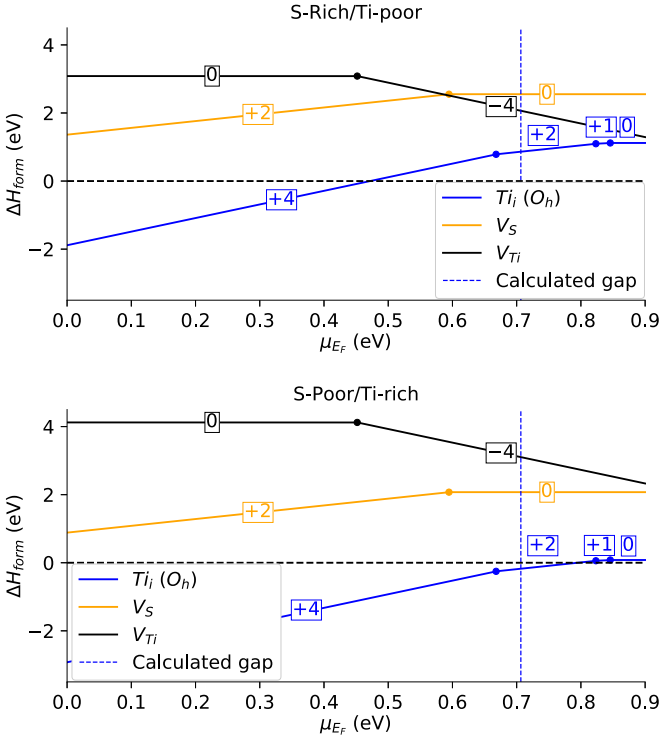


FIG. 4. $TiS_2$ defect formation enthalpies computed with dispersion corrected hybrid functional PBE0-GD3BJ vs Fermi level for $Ti_i$ (blue), $V_S$ (orange), and $V_{Ti}$ (black). For each defect, only the lowest formation enthalpy of all possible states of charge is displayed for clarity. The slope of the line is the charge, indicated in the small frames. The charge of lowest enthalpy depends on the Fermi level. Transition levels mark Fermi level values at which the charge changes. They are highlighted by circles in the figure.

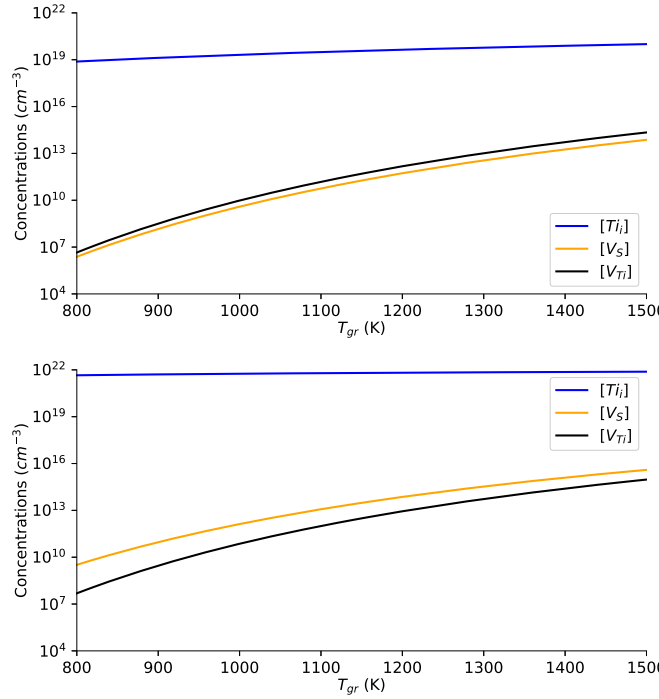


FIG. 5. $TiS_2$ defect concentrations vs growth temperature (top: S-rich/Ti-poor, bottom: S-poor/Ti-rich).

conditions. The transition level $\epsilon_{(+2,0)}$ shows up at $-0.11$ eV from the CBM ($\mu_{E_F} = \epsilon_{(+2,0)} = 0.60$ eV) thus $V_S$ is a shallow donor. The formation cost is smaller in S-poor/Ti-rich conditions but remains important ($\Delta H^{V_S}_{\text{form}}(\epsilon_{(+2,0)}) = 2.07$ eV).

The case of $Ti_i$ is more intricated. In S-rich/Ti-poor conditions, the formation enthalpy of $Ti_i$ is negative until $\mu_{E_F} = 0.47$ eV and $Ti_i$ exhibits a shallow transition level $\epsilon_{(+4,+2)}$ 0.04 eV below the conduction-band minimum (CBM). The oxidation state +III does not appear in thermodynamical conditions due to a negative $U$ behavior [101] (see Fig. 1 of the Supplemental Material for defect formation enthalpies [92]). A negative defect formation enthalpy means that the point defect is so easy to create that many defects will form spontaneously and destabilize the host, leading to the formation of another phase (at least for $\Delta H \ll 0$). Hole conductivity is thus impossible for the following reasons. First, the $p$-type doping limit of $TiS_2$ dopability domain is set by $\Delta H^{Ti_i}_{\text{form}}(\mu_{E_F}) = 0$, far above the VBM. Second, the acceptor $V_{Ti}$ has a very high formation enthalpy as aforementioned, and a deep transition level. These facts demonstrate that a hole conductivity ($p$-type) is clearly impossible for the bulk material.

In S-poor/Ti-rich conditions, the results concerning $Ti_i$ are slightly puzzling. According to our results at the PBE0-GD3BJ level of theory, the defect formation enthalpy is always negative in the whole range of $\mu_{E_F}$. Therefore, either the Fermi level remains inferior to the band gap, resulting in the decomposition of $TiS_2$ into another phase, or the Fermi level enters the conduction band leading to a $Ti_i^{2+}$ and a degenerate semiconducting/(semi)metallic $TiS_2$.

In both growth conditions, a transition level $\epsilon_{(+4,+2)}$ lies very close to the CBM ($-0.04$ eV, $\mu_{E_F} = 0.67$ eV), making $Ti_i$ a very shallow defect. Because of the sign of $\Delta H^{Ti_i}_{\text{form}}$ in the band gap, this leads to a strong $n$-type semiconductor in the S-rich/Ti-poor atmosphere and a degenerate semiconductor/(semi)metal in the other case.

### E. Defect concentrations

When comparing different defects, the ones having a higher formation enthalpy require more energy to appear, and consequently will be found at lower concentrations in the material. Defect concentrations will be determined by the synthesis atmosphere and temperature (quenching hypothesis).

The mobilities of electrons and holes are high and of the same order of magnitude. This allows us to evaluate defect concentrations vs synthesis temperature $T_{\text{gr}}$, as shown in Fig. 5. The concentrations for two realistic synthesis temperatures $T_{gr} = 900$ K and $T_{gr} = 1200$ K are reported in Table II. In a S-rich/Ti-poor atmosphere, $[Ti_i] \simeq 10^{19}$ cm$^{-3}$and in S-poor/Ti-rich atmosphere, $[Ti_i] \simeq 10^{21}$ cm$^{-3}$. In a S-rich/Ti-poor atmosphere, $V_{Ti}$ is slightly more present than $V_S$ while in a S-poor/Ti-rich atmosphere, it is the opposite, coherently with the atmospheres. These calculated orders of magnitude reflect well a material which is reported to get easily off-stoichiometry. The charges introduced by such defects are balanced by the apparition of free charge carriers at room temperature, mainly electrons, due to a thermally assisted transition from the VB to the CB. We obtain $n_{e^-} \simeq 10^{18}$ cm$^{-3}$ in S-rich/Ti-poor and $n_{e^-} \simeq 10^{20}$ cm$^{-3}$ in S-poor/Ti-rich,

TABLE II. Defect concentrations ($cm^{-3}$) vs growth temperature and atmosphere.

| | $Ti_i$ | $V_S$ | $V_{Ti}$ |
|---|---|---|---|
| S-rich/Ti-poor ($T_{gr} = 900$ K) | $1.3 \times 10^{19}$ | $1.4 \times 10^{8}$ | $3.2 \times 10^{9}$ |
| S-rich/Ti-poor ($T_{gr} = 1200$ K) | $4.4 \times 10^{19}$ | $5.3 \times 10^{11}$ | $1.5 \times 10^{12}$ |
| S-poor/Ti-rich ($T_{gr} = 900$ K) | $5.1 \times 10^{21}$ | $9.2 \times 10^{10}$ | $2.9 \times 10^{9}$ |
| S-poor/Ti-rich ($T_{gr} = 1200$ K) | $9.1 \times 10^{21}$ | $8.5 \times 10^{13}$ | $1.0 \times 10^{13}$ |

vs $n_{h^+} \simeq 10^{12}$ $cm^{-3}$ in S-rich, $n_{h^+} \simeq 10^{9}$ $cm^{-3}$ in S-poor, respectively. These values match the experimental value of charge concentrations of $\approx 10^{20}$ $cm^{-3}$ [21].

### F. Origin of the versatile behavior of $TiS_2$

Intuitively, the concentration of $Ti_i$ increases with $\mu_{Ti}$ (as $|\Delta\mu_{Ti}|$ decreases). The richer the titanium atmosphere the more concentrated the titanium interstitials are. Going from S-rich/Ti-poor to S-poor/Ti-rich synthesis conditions, the Fermi level will move from just above the donor level to somewhere in the bottom of the conduction band. The limit case where $E_F^{gr}$ hits the CBM corresponds to the frontier between the nondegenerate semiconducting behavior (SC) and the degenerate semiconducting/semimetallic one (SM).

This led us to investigate where this transition happens in the stability domain. Let us define as $\alpha$ the progression parameter from S-rich/Ti-poor to S-poor/Ti-rich. When $\alpha = 0$, the synthesis conditions are such that the chemical potentials are set to the S-rich/Ti-poor limit investigated previously (semiconductor). When $\alpha = 1$, they are set to the S-poor/Ti-rich limit (degenerate/metallic). Formally, for $X \in \{Ti, S\}$, $\mu_X^{\alpha} = (1-\alpha)\mu_X^{\text{Ti-poor}} + \alpha\mu_X^{\text{Ti-rich}}$.

For any $\alpha \in [0; 1]$, one can calculate as before the Fermi level $E_F^{gr}(T_{gr}, \alpha)$ at a given growth temperature $T_{gr}$. For a range of $T_{gr}$, we can now solve the equation in $\alpha$ $E_F^{gr}(T_{gr}, \alpha) = E_g$ to obtain the position of the frontier between semiconducting and (semi)metallic behaviors (see Fig.6).

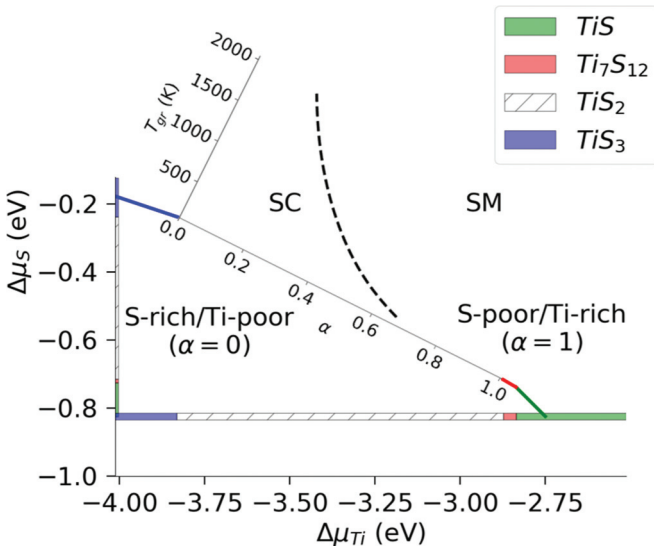


FIG. 6. $TiS_2$ temperature of semiconductor/(semi)metal transition vs synthesis conditions shown in the stability domain as a function of the progression $\alpha$ from the S-rich/Ti-poor limit ($\alpha = 0$) to the S-poor/Ti-rich one ($\alpha = 1$). For a given position in $TiS_2$ stability domain $\alpha$, the corresponding chemical potentials can be read on the main $x$ ($\Delta\mu_{Ti}$) and y ($\Delta\mu_S$) axis.

For low synthesis temperatures, disorder (defect formations) is inhibited, thus the semiconducting domain is the largest ($\alpha \simeq 0.63$ at $T_{gr} \simeq 300$ K). When the temperature increases, disorders are more likely to happen and the frontier moves towards the S-rich/Ti-poor limit. A fitting shows a cubic behavior [$T_{gr} = (1-\alpha)^3$] for the frontier. At this point, one should recall that the stability domain is 0.95 eV wide on the $\Delta\mu_{Ti}$ axis and 0.48 eV wide on the $\Delta\mu_S$ axis all in all. Besides, the S atmosphere is experimentally very difficult to control. This explains why it is possible to obtain experimentally a semiconducting (nondegenerate) and semimetallic behavior for $TiS_2$.

## V. CONCLUSION

The electronic properties of $TiS_2$ led to controversies in the past. In a previous study, we found that the hybrid functional (PBE0) including dispersion corrections was the method currently presenting the best ratio of accuracy over computational time to describe correctly $TiS_2$. We concluded that ideal stoichiometric $TiS_2$ is a small gap semiconductor.

The analysis of the stability domain enlightens the difficulty to obtain stoichiometric $TiS_2$. Calculated defect formation enthalpies clearly point to $Ti_{i(O_h)}$ as the major defect in $TiS_2$ by far. It drives $n$-type conductivity in the material. According to our calculations in the thermodynamic limit, $V_S$ and $V_{Ti}$ are found only in tiny amounts.

Our calculations showed that in S-rich/Ti-poor conditions, the synthesis of $TiS_2$ leads to a nondegenerate semiconductor with a strong electron conductivity. In contrast in S-poor/Ti-rich conditions, it leads to a degenerate semiconductor exhibiting (semi)metallic properties: because of the very low formation enthalpy of $Ti_i$, in S-poor/Ti-rich conditions the Fermi level must enter the CB to not destabilize the host into a new phase.

This study confirms the experimental hypothesis of $Ti_i$ being the majority defect (even in Ti-poor synthesis conditions). It shows that, in addition to the difficulty to obtain stoichiometric $TiS_2$, its electronic properties are very sensitive to defects and that a small amount of titanium spontaneously inserting themselves in the van der Waals gap is enough to switch from semiconductor to semimetal.

## ACKNOWLEDGMENTS

A.S. thanks the CNRS and Region des Pays de Loire for financial support. The CCIPL (Centre de Calcul Intensif des Pays de Loire) is acknowledged for computational resources.

[1] J. Rouxel, J. Solid State Chem. **64**, 305 (1986).
[2] Q. H. Wang, K. Kalantar-Zadeh, A. Kis, J. N. Coleman, and M. S. Strano, Nat. Nanotechnol. **7**, 699 (2012).
[3] M. M. Ugeda, A. J. Bradley, S. F. Shi, F. H. Da Jornada, Y. Zhang, D. Y. Qiu, W. Ruan, S. K. Mo, Z. Hussain, Z. X. Shen, F. Wang, S. G. Louie, and M. F. Crommie, Nat. Mater. **13**, 1091 (2014).
[4] K. F. Mak and J. Shan, Nat. Photon. **10**, 216 (2016).
[5] M. Kelly, *Low-dimensional Semiconductors: Materials, Physics, Technology, Devices*, Series on Semiconductor Science and Technology (Clarendon, Oxford, 1995).
[6] K. Barnham and D. Vvedensky, *Low-Dimensional Semiconductor Structures: Fundamentals and Device Applications* (Cambridge University Press, Cambridge, UK, 2008).
[7] G. Fiori, F. Bonaccorso, G. Iannaccone, T. Palacios, D. Neumaier, A. Seabaugh, S. K. Banerjee, and L. Colombo, Nat. Nanotechnol. **9**, 768 (2014).
[8] A. Jayakumar, A. Surendranath, and M. PV, Int. J. Pharm. **551**, 309 (2018).
[9] P. Bollella, G. Fusco, C. Tortolini, G. Sanzò, G. Favero, L. Gorton, and R. Antiochia, Biosens. Bioelectron. **89**, 152 (2017).
[10] T. Zhang, J. Liu, C. Wang, X. Leng, Y. Xiao, and L. Fu, Biosens. Bioelectron. **89**, 28 (2017).
[11] H. Tang, Q. Hu, M. Zheng, Y. Chi, X. Qin, H. Pang, and Q. Xu, Prog. Nat. Sc.: Mater. Int. **28**, 133 (2018).
[12] N. Jiang, B. Li, F. Ning, and D. Xia, J. Energy Chem. **27**, 1651 (2018).
[13] Y. Yang, X. Liu, Z. Zhu, Y. Zhong, Y. Bando, D. Golberg, J. Yao, and X. Wang, Joule **2**, 1075 (2018).
[14] J. Wilson and A. Yoffe, Adv. Phys. **18**, 193 (1969).
[15] J. A. Benda, Phys. Rev. B **10**, 1409 (1974).
[16] G. Lucovsky, R. M. White, J. A. Benda, and J. F. Revelli, Phys. Rev. B **7**, 3859 (1973).
[17] F. R. Shepherd and P. M. Williams, J. Phys. C **7**, 4416 (1974).
[18] A. H. Thompson, K. R. Pisharody, and R. F. Koehler, Phys. Rev. Lett. **29**, 163 (1972).
[19] A. Zunger and A. J. Freeman, Phys. Rev. B **16**, 906 (1977).
[20] F. C. Brown, Physica B&C (Amsterdam) **99**, 264 (1980).
[21] E. M. Logothetis, W. J. Kaiser, C. A. Kukkonen, S. P. Faile, R. Colella, and J. Gambold, Physica B&C (Amsterdam) **99**, 193 (1980).
[22] M. Inoue, H. Negishi, and S. Sonokawa, Z. Phys. B **67**, 319 (1987).
[23] Z. Wu, F. Lemoigno, P. Gressier, G. Ouvrard, P. Moreau, J. Rouxel, and C. R. Natoli, Phys. Rev. B **54**, R11009 (1996).
[24] S. Surampudi, D. Shen, C.-K. Huang, F. Deligiannis, A. Attia, and G. Halpert, J. Power Sources **36**, 395 (1991).
[25] D. Cherns and G. Ngo, J. Solid State Chem. **50**, 7 (1983).
[26] B. Knutz and S. Skaarup, Solid State Ionics **9-10**, 371 (1983).
[27] C. Julien, O. Gorochov, and A. Ghorayeb, Mater. Sci. Eng., B **14**, 418 (1992).
[28] J. Wang, Solid State Ionics **40-41**, 548 (1990).
[29] P. Moreau, G. Ouvrard, P. Gressier, P. Ganal, and J. Rouxel, J. Phys. Chem. Solids **57**, 1117 (1996).
[30] H. Brauer, H. Starnberg, L. Holleboom, and H. Hughes, Surf. Sci. **331-333**, 419 (1995).
[31] M. Remškar, A. Popović, and H. Starnberg, Surf. Sci. **430**, 199 (1999).
[32] T. E. Sutto and T. T. Duncan, Electrochim. Acta **77**, 204 (2012).
[33] P. Moreau, P. Ganal, S. Lemaux, G. Ouvrard, and M. McKelvy, J. Phys. Chem. Solids **57**, 1129 (1996).
[34] G. Ouvrard and D. Guyomard, Curr. Opin. Solid State Mater. Sci. **1**, 260 (1996).
[35] T. Butz, R.-H. Flagmeyer, S. Jankuhn, T. Reinert, M. da Silva, J. Soares, and W. Tröger, Nucl. Instrum. Methods Phys. Res., Sect. B **136-138**, 253 (1998).
[36] M. Sidorov, M. McKelvy, R. Sharma, W. Glaunsinger, P. Ganal, P. Moreau, and G. Ouvrard, Chem. Mater. **7**, 1140 (1995).
[37] P. Ganal, P. Moreau, G. Ouvrard, M. Sidorov, M. McKelvy, and W. Glaunsinger, Chem. Mater. **7**, 1132 (1995).
[38] P. Moreau, P. Ganal, and G. Ouvrard, Mol. Cryst. Liq. Cryst. Sci. Technol., Sect. A **244**, 325 (1994).
[39] *Chemical Physics of Intercalation II*, edited by P. Bernier *et al.* (Plenum Press, New York, 1993).
[40] M. J. Smith and C. A. Vincent, J. Chem. Thermodyn. **18**, 1183 (1986).
[41] J. Heitmann, J. McCallum, W. Tröger, and T. Butz, Nucl. Instrum. Methods Phys. Res., Sect. B **158**, 689 (1999).
[42] J. Heitmann, J. McCallum, W. Tröger, T. Butz, and R. Hesse, Nucl. Instrum. Methods Phys. Res., Sect. B **161-163**, 619 (2000).
[43] S. Li, J. Liu, and B. Liu, J. Power Sources **320**, 322 (2016).
[44] P. Lavela, J. Morales, and J. Tirado, J. Solid State Chem. **124**, 238 (1996).
[45] C. Papageorgopoulos, M. Kamaratos, D. Papageorgopoulos, D. Tonti, C. Pettenkofer, and W. Jaegermann, Surf. Sci. **436**, 213 (1999).
[46] X. Cao, Y. Tang, J. Ø. Duus, and Q. Chi, in *Handbook of Ecomaterials*, edited by L. M. T. Martínez, O. V. Kharissova, and B. I. Kharisov (Springer International Publishing, Cham, 2017), pp. 1–29.
[47] J. Chen, S.-L. Li, Z.-L. Tao, Y.-T. Shen, and C.-X. Cui, J. Am. Chem. Soc. **125**, 5284 (2003).
[48] H. Imai, Y. Shimakawa, and Y. Kubo, Phys. Rev. B **64**, 241104 (2001).
[49] J. Zhang, X. Y. Qin, D. Li, H. X. Xin, L. Pan, and K. X. Zhang, J. Alloys Compd. **479**, 816 (2009).
[50] E. Guilmeau, Y. Bréard, and A. Maignan, Appl. Phys. Lett. **99**, 052107 (2011).
[51] C. Bourgès, T. Barbier, G. Guélou, P. Vaqueiro, A. V. Powell, O. I. Lebedev, N. Barrier, Y. Kinemuchi, and E. Guilmeau, J. Eur. Ceram. Soc. **36**, 1183 (2015).
[52] M. J. McKelvy and W. S. Glaunsinger, J. Solid State Chem. **66**, 181 (1987).
[53] B. Liu, J. Yang, C. Liu, T. Hu, Y. Han, and C. Gao, Phys. Status Solidi C **8**, 1683 (2011).
[54] Q. Yan-Bin, Z. Guo-Hua, L. Di, W. Jiang-Long, Q. Xiao-Ying, and Z. Zhi, Chin. Phys. Lett. **24**, 1050 (2007).
[55] F. Güller, C. Helman, and A. Llois, Physica B (Amsterdam) **407**, 3188 (2012).
[56] A. V. Bandura and R. A. Evarestov, J. Comput. Chem. **35**, 395 (2014).
[57] V. D. S. Ganesan, C. Zhang, Y. P. Feng, and L. Shen, arXiv:1507.07343.
[58] B. Liu, J. Yang, Y. Han, T. Hu, W. Ren, C. Liu, Y. Ma, and C. Gao, J. Appl. Phys. **109**, 053717 (2011).

[59] C. Xu, P. A. Brown, and K. L. Shuford, RSC Adv. **5**, 83876 (2015).

[60] D. Zhou, Y. Xu, L. Bai, B. Shen, X. Wang, Y. Zou, and J. Tian, J. Alloys Compd. **757**, 448 (2018).

[61] H. Kasai, K. Tolborg, M. Sist, J. Zhang, V. R. Hathwar, M. Filsø, S. Cenedese, K. Sugimoto, J. Overgaard, E. Nishibori, and B. B. Iversen, Nat. Mater. **17**, 249 (2018).

[62] Q. Song, Z. Wu, P. Ma, G. Wang, and B. Zhang, Infrared Phys. Technol. **92**, 1 (2018).

[63] M. Parvaz, N. A. Salah, and Z. H. Khan, Optik **171**, 183 (2018).

[64] N. Dhenadhayalan, M. I. Sriram, and K.-C. Lin, Sens. Actuators B: Chemical **258**, 929 (2018).

[65] W. Choi, N. Choudhary, G. H. Han, J. Park, D. Akinwande, and Y. H. Lee, Mater. Today **20**, 116 (2017).

[66] P. Srimuk, J. Lee, A. Tolosa, C. Kim, M. Aslan, and V. Presser, Chem. Mater. **29**, 9964 (2017).

[67] A. Stoliaroff, S. Jobic, and C. Latouche, Inorg. Chem. **58**, 1949 (2019).

[68] F. Oba, A. Togo, I. Tanaka, J. Paier, and G. Kresse, Phys. Rev. B **77**, 245202 (2008).

[69] A. Goyal, P. Gorai, E. S. Toberer, and V. Stevanovic, npj Comput. Mater. **3**, 42 (2017).

[70] H. M. Widatallah, M. S. Al-Barwani, E. A. Moore, and M. E. Elzain, J. Phys. Chem. Solids **119**, 100 (2018).

[71] E. Igumbor, O. Olaniyan, R. Mapasha, H. Danga, E. Omotoso, and W. Meyer, Mater. Sci. Semicond. Process. **89**, 77 (2019).

[72] V. Çelik and E. Mete, Comput. Condens. Matter **16**, e00307 (2018).

[73] J. C. Mikkelsen, Nuovo Cimento B **38**, 378 (2007).

[74] J. P. Perdew, K. Burke, and M. Ernzerhof, Phys. Rev. Lett. **77**, 3865 (1996).

[75] J. Paier, R. Hirschl, M. Marsman, and G. Kresse, J. Chem. Phys. **122**, 234102 (2005).

[76] G. Kresse and J. Hafner, Phys. Rev. B **47**, 558 (1993).

[77] G. Kresse and J. Hafner, Phys. Rev. B **49**, 14251 (1994).

[78] G. Kresse and J. Furthmüller, Comput. Mater. Sci. **6**, 15 (1996).

[79] G. Kresse and J. Furthmüller, Phys. Rev. B **54**, 11169 (1996).

[80] S. Grimme, J. Antony, S. Ehrlich, and H. Krieg, J. Chem. Phys. **132**, 154104 (2010).

[81] S. Grimme, S. Ehrlich, and L. Goerigk, J. Comput. Chem. **32**, 1456 (2011).

[82] A. D. Becke and E. R. Johnson, J. Chem. Phys. **127**, 154108 (2007).

[83] H. J. Monkhorst and J. D. Pack, Phys. Rev. B **13**, 5188 (1976).

[84] E. Péan, J. Vidal, S. Jobic, and C. Latouche, Chem. Phys. Lett. **671**, 124 (2017).

[85] A. Stoliaroff, S. Jobic, and C. Latouche, J. Comput. Chem. **39**, 2251 (2018).

[86] F. Oba, M. Choi, A. Togo, and I. Tanaka, Sci. Technol. Adv. Mater. **12**, 34302 (2011).

[87] S. Lany and A. Zunger, Phys. Rev. B **78**, 235104 (2008).

[88] S. Lany and A. Zunger, Modell. Simul. Mater. Sci. Eng. **17**, 084002 (2009).

[89] C. Freysoldt, B. Grabowski, T. Hickel, J. Neugebauer, G. Kresse, A. Janotti, and C. G. Van de Walle, Rev. Mod. Phys. **86**, 253 (2014).

[90] J. L. Lyons and C. G. V. de Walle, npj Comput. Mater. **3**, 12 (2017).

[91] A. F. Kohan, G. Ceder, D. Morgan, and C. G. V. d. Walle, Phys. Rev. B **61**, 15019 (2000).

[92] See Supplemental Material at http://link.aps.org/supplemental/10.1103/PhysRevB.99.165122 for a description of the energy corrections in the point defect model, stability domain equations, and defect formation enthalpies (see Refs. [102–104]).

[93] R. Chianelli, J. Scanlon, and A. Thompson, Mater. Res. Bull. **10**, 1379 (1975).

[94] M. Hellenbrandt, Crystallogr. Rev. **10**, 17 (2004).

[95] ICSD crystallographic database, http://www2.fiz-karlsruhe.de/Icsd_home.html?&L=, accessed: 2018/12/12 .

[96] A. Jain, S. P. Ong, G. Hautier, W. Chen, W. D. Richards, S. Dacek, S. Cholia, D. Gunter, D. Skinner, G. Ceder, and K. A. Persson, APL Mater. **1**, 011002 (2013).

[97] S. P. Ong, L. Wang, B. Kang, and G. Ceder, Chem. Mater. **20**, 1798 (2008).

[98] A. Jain, G. Hautier, S. Ong, C. Moore, C. Fischer, K. Persson, and G. Ceder, Phys. Rev. B **84**, 045115 (2011).

[99] J. L. Murray, Bull. Alloy Phase Diagrams **7**, 156 (1986).

[100] E. Tronc, R. Moret, J. J. Legendre, and M. Huber, Acta Crystallogr. Sect. B **31**, 2800 (1975).

[101] Y. Kumagai and F. Oba, Phys. Rev. B **89**, 195205 (2014).

[102] E. Burstein, Phys. Rev. **93**, 632 (1954).

[103] T. S. Moss, Proc. Phys. Soc. London, Sect. B **67**, 775 (1954).

[104] Y. Quéré, *Physique des matériaux: cours et problèmes*, edited by P. Ellipses (1988).